Title

Large-scale identification of plasma membrane repair proteins revealed spatiotemporal cellular responses to plasma membrane damage

Authors

Yuta Yamazaki[1] and Keiko Kono[1]*

Affiliations

1 Okinawa Institute of Science and Technology Graduate University, 1919-1 Tancha, Onna, Okinawa, 904-0495, Japan

* Corresponding author. E-mail: keiko.kono@oist.jp (K.K.)

Abstract

Damage to the plasma membrane (PM) is common in all types of cells. PM repair processes, including exocytosis and endocytosis, are not mutually exclusive; rather, they collaborate to repair the wound. However, the temporal coordination between the repair processes remains poorly understood. Here, by large-scale identification and live-cell imaging of PM repair proteins, we analyzed the spatiotemporal PM damage responses in *Saccharomyces cerevisiae*. Of the 80 repair proteins identified, 72 proteins were previously unreported repair protein candidates. Among the observed repair processes, the polarized exocytosis and clathrin-mediated endocytosis (CME) are coupled at the damage site, with exocytosis predominating in the early stage of PM repair and CME predominating in the late stage of PM repair. Furthermore, we showed that CME at the growing bud site directs PM repair proteins with transmembrane domains to the damage site. We propose a model in which CME delivers repair proteins with transmembrane domains between the growing bud site and the damage site. This study provides a functional catalog of PM repair proteins and insights into spatiotemporal cellular responses to PM damage.

Introduction

The plasma membrane (PM) functions as a defensive barrier in all types of cells to protect cellular components from extracellular stimuli. PM frequently experiences physiological and pathological damages, such as eccentric contraction-induced injuries, migration-induced injuries, pore formation by bacterial toxins, or invasion by cancer cells (1, 2). Cells undergo cell lysis if the damaged PM is not repaired. Deficits in PM repair are linked to multiple diseases, including limb-girdle muscular dystrophy (3) and Scott syndrome (4, 5). Therefore, virtually all cells have PM repair machinery.

In eukaryotes, the influx of Ca^{2+} triggers PM repair (1). Upon Ca^{2+} influx, fundamental cellular mechanisms, including exocytosis (6-10), endocytosis (11, 12), membrane shedding by ESCRT complex (13, 14), and the constriction forces by actin cytoskeleton (15-18) are directed to the damage site to reseal the wound. These initial repair processes usually occur within 1 min after PM damage (19). After the resealing of the damaged PM, cells restructure the damaged PM (19-21). Restructuring is defined as the process by which cells modify the damaged PM to restore PM homeostasis and normal cell function (19-21). These repair processes are not mutually exclusive, and they collaborate to repair the damaged PM (22). However, the temporal coordination between the PM repair processes remains poorly understood.

Both resealing and restructuring of the damaged PM are mediated by the proteins, which accumulate at the damage site. Here, we defined them as PM repair proteins. PM repair proteins include ESCRT, annexins, and dysferlin in mammalian cells (13, 23-25). Using budding yeast *Saccharomyces cerevisiae* as a model, we previously identified evolutionarily conserved repair proteins, including protein kinase C, exocyst, and phospholipid flippases (26, 27). These repair proteins accumulate at the damage site at the appropriate time and proceed with the repair processes. Therefore, identifying repair proteins and observing their movements after PM damage is an important step toward understanding the temporal PM repair processes.

Here, we performed proteome-scale screening of PM repair proteins using yeast GFP-tagged libraries and laser-induced injury assay in budding yeast. We identified 80 repair protein candidates, including 72 previously unreported candidates. Among the observed repair processes, we showed that polarized exocytosis and clathrin-mediated endocytosis (CME) are coupled at the damage site, with exocytosis predominating in the early stage of PM repair and CME predominating in the late stage of PM repair. We also showed that CME delivers repair proteins with transmembrane domains (TMDs) from the growing bud site (bud tip) to the damage site, presumably contributing to the restructuring of the damaged PM. These results provide insights into the temporal dynamics of coordinated cellular responses to PM damage.

Results

Proteome-scale identification of PM/cell wall damage-responsive proteins

To identify the PM repair proteins, we performed a two-step screening. First, we aimed to identify the proteins that change localization in response to SDS treatment, which induces local PM/cell wall damage to budding yeast (28). We used a yeast C-terminally GFP-tagged library (4159 ORFs) (29) and an N-terminally sfGFP-tagged library (N' Swat library) (5569 ORFs) (30, 31) comprising 86% of the yeast proteome (5718 ORFs in total) (Fig. 1A). We fixed the cells with paraformaldehyde after 1 hour of SDS treatment, in which condition the best-characterized repair protein Pkc1-GFP changes its localization (Fig. 1A). We successfully imaged the signal of 9181 proteins fused with GFP or sfGFP (5609 ORFs in total). We assessed the fluorescence signals of 5609 proteins in normal and SDS-treated conditions by visual inspection of the images. We identified 562 proteins whose fluorescence signal pattern changed after SDS treatment (Fig. 1B and Data S1). The hits included the localization changes of proteins, structural changes of organelles such as mitochondrial fragmentation, and foci/puncta formation in response to SDS treatment. In addition to Pkc1, we identified previously reported repair proteins, such as Rom2

and Dnf1, as screening hits (26, 27) (Data S1). Gene Ontology (GO) analysis of the screening hits revealed enrichment for proteins involved in the actin filament organization (Fig. 1C). This is consistent with the previous study that SDS treatment remodels the cell polarity and actin cytoskeleton (26). Based on the reported subcellular localization of proteins, we categorized the screening hits into six major classes and several minor ones representing less than ten proteins (Fig. 1D and fig. S1, see Materials and Methods). Among the hits, proteins that are localized to the cell periphery showed cytoplasmic dots after SDS treatment (Fig. 1D). This is consistent with the fact that endocytosis of PM proteins contributes to cell adaptation to environmental stress (32). We also found that proteins that form puncta/foci after the SDS treatment include translation factor Gcd7-GFP (Fig. 1D), which forms foci in response to glucose deprivation (33). These observations suggest that SDS treatment induces stress responses, including those associated with PM/cell wall damage responses in budding yeast.

Laser-induced PM/cell wall damage assay identified 80 repair protein candidates

Our group previously developed a laser-induced PM/cell wall injury assay under live single-cell conditions (laser damage assay) (26, 34). We performed the laser damage assay to identify the PM repair proteins and observe their movements after PM/cell wall damage (Fig. 2A). The N-terminally sfGFP-tagged library is expressed under exogenous *NOP1* promoters, while the C-terminally GFP-tagged library is expressed under endogenous promoters (29, 30). To assess the proteins with endogenous expression levels, we selected the 234 screening hits from the C-terminal library as targets for the laser damage assay. During 25 min of observation at 30-second intervals, we identified 90 proteins whose localization changed in response to laser damage (Fig. 2B). We categorized the proteins into four classes based on their localization changes (Fig. 2C). Three of the puncta-forming proteins, Dna2, Dot6, and Gcd7, form puncta in response to cellular stresses (33, 35). In addition, the transcription factors, Msn2 and Crz1, translocate from the cytoplasm to the nucleus after laser damage (Fig. 2B). Msn2 and Crz1 are activated under various stress conditions (36). Thus, the localization changes of puncta-forming proteins and transcriptional factors suggest common stress responses to laser damage and other cellular stresses. The most frequently observed localization changes were the accumulation at the damage site (Fig. 2B). We defined them as repair protein candidates, given their presumed involvement in the PM/cell wall repair process.

To gain further insight into the repair protein candidates, we classified them into four categories based on their subcellular localization (Fig. 2C). The largest category is bud-localized proteins (47 proteins) (Fig. 2C), which is consistent with a previous study showing that bud-localized proteins accumulate at the damage site in budding yeast (26). The repair protein candidates in this category include ten proteins that have transmembrane domains (TMDs), including phospholipid flippases (Dnf1/Dnf2) and osmosensor proteins (Slg1, Sho1) (Fig. 2C). Proteins with TMDs are transported to the PM as cargoes of secretory vesicles (37). Thus, this result suggests that secretory vesicles targeted to the damage site provide repair proteins with TMDs to the damage site. The second largest category is actin-localized proteins (25 proteins). This is consistent with the GO analysis that actin-binding proteins and proteins involved in actin-related biological processes are enriched in the repair protein candidates (Fig. 2, D and E). The proteins in this category include endocytic proteins, suggesting that endocytosis occurs at the damage site. In addition, proteins that bind actin cables, such as Abp140, are included in this category, suggesting that actin cables are formed at the damage site. These results are consistent with previous studies of PM damage repair in budding yeast and human cells (11, 26).

The temporal order of the Pkc1 accumulation, polarized exocytosis, and CME at the damage site

147 To understand when repair proteins accumulate at the damage site, we defined their accumulation
148 times as the time when the fluorescence intensity at the damage site exceeded the threefold
149 standard deviation (3xSD) above the non-damaged site for at least two consecutive time frames (1
150 min). We also defined dispersion time when the fluorescence intensity at the damage site becomes
151 less than that of the non-damaged site plus 3xSD for at least 1 min (Data S2).
152 The defined accumulation times raised the possibility that the Pkc1 pathway proteins accumulated
153 at the damage site earlier than exocytosis regulators and exocytic cargoes with transmembrane
154 domains (Dnf1, Dnf2, and Slg1) (Fig. S2). To verify this observation, we performed the laser
155 damage assay in the cells expressing Exo70-mNeonGreen (mNG) and Pkc1-mScarlet-I (mSc-I),
156 and the cells expressing Pkc1-sfGFP and Dnf1-mSc-I (Fig. 3A and B). Exo70 is one of the
157 subunits of the exocyst complex, serving as a polarized exocytosis marker. The fluorescence-
158 tagged Pkc1 accumulated at the damage site earlier than Exo70-mNG and Dnf1-mSc-I (Fig. 3, A
159 and B). These results suggest that the Pkc1 accumulation at the damage site occurs earlier than the
160 polarized exocytosis of transmembrane proteins.
161 Although not all exocyst subunits (eight subunits) were identified in this work, all the mSc-I-
162 tagged exocyst subunits showed comparable fluorescence intensity changes with Exo70-mNG at
163 the damage site and at the bud tip (Fig. S3, A to G). These results suggest that all subunits of the
164 exocyst complex accumulate at the damage site simultaneously.
165 The CME markers, Sla1-GFP and Abp1-GFP (38), exhibited repeated short stays and
166 reaccumulation at the damage site within 5 min to 25 min after laser damage (Fig. S4, A to C).
167 These fluctuating movements of Sla1 and Abp1 are consistent with the previous studies (39, 40).
168 Furthermore, Sla1-mNG and Abp1-mSc-I showed comparable fluctuating accumulation patterns
169 in the same cell (Fig. S4D). These results suggest that CME repeatedly occurs at the damage site
170 from around 5 min to 25 min after laser damage.
171 To understand the temporal order of polarized exocytosis and CME at the damage site, we
172 performed the laser damage assay in the cells expressing Exo70-mNG/Dnf1-mNG and Ede1-
173 mSc-I (Fig. 3, C and D). Ede1 is one of the earliest proteins recruited to endocytic sites, serving
174 as a CME marker (41, 42). Exo70-mNG/Dnf1-mNG and Ede1-mSc-I simultaneously
175 accumulated at the damage site from 5 min to 35 min (Fig. 3, C and D). The signals of Exo70-
176 mNG/Dnf1-mNG peak within 20 min after the damage, while Ede1-mSc-I peaks 20 min after the
177 damage (Fig. 3, C and D). These results suggest that CME and polarized exocytosis occur
178 simultaneously at the damage site, with polarized exocytosis predominating in the early stage of
179 the PM/cell wall damage response and CME predominating in the late stage of the PM/cell wall
180 damage response.
181
182 **Knockout mutants of CME are sensitive to PM/cell wall stresses**
183 To identify the biological processes required for cell survival after PM/cell wall stress, we
184 performed growth screening of repair protein knockout mutants in PM/cell wall stress conditions
185 (Fig. S5A). We spotted the same number of yeast cells in YPD media, YPD+0.01% SDS media,
186 YPD+25 µg/ml calcofluor white (CFW), and YPD media in 37 °C (Heat stress) and incubated for
187 3 days (Fig. S5A). CFW binds to chitin in the cell wall, inducing cell wall damage (43). Heat
188 stress modifies PM structures (44). The growth assay showed that six knockout mutants of CME
189 proteins, *rvs167*Δ, *sla1*Δ, *sla2*Δ, *end3*Δ, *las17*Δ, and *vrp1*Δ, are sensitive to all the stress
190 conditions (Fig. S5B). We knocked out these genes using the WT strain in our laboratory and
191 confirmed that these mutants are sensitive to SDS (Fig. S5C). These results led us to focus further
192 on the CME functions associated with PM/cell wall damage repair.
193
194 **CME proteins are required for polarized exocytosis at the damage site**
195 Previous studies showed that endocytosis is involved in PM damage repair by directly resealing
196 the PM by removing the damaged pores (45) or by restructuring the PM after resealing in

197 mammalian cells (20, 21, 46). We showed that CME occurs at the damage site from 5 to 45 min
198 after laser damage in budding yeast (Fig. 3, B and C). This supports the possibility that CME
199 restructures the PM after resealing, which usually occurs within 1 min after the damage (20).
200 Another potential mechanism for restructuring the damaged PM is exocytosis, which delivers PM
201 proteins and lipids to the damage site. Our previous work showed that the polarized exocytosis
202 machinery is directed from the bud tip to the damage site in response to laser damage in budding
203 yeast (26). Given that CME and polarized exocytosis constitute a coupled transport cycle in
204 budding yeast (47), we reasoned that CME positively regulates polarized exocytosis at the
205 damage site, thereby restructuring the damaged PM.
206 To test this idea, we performed the laser damage assay in SDS-sensitive endocytic mutants
207 (*sla1*Δ, *end3*Δ, *vrp1*Δ, and *rvs167*Δ). We used two exocytosis markers, type V myosin (Myo2)
208 and the exocyst subunit (Exo70), fused to sfGFP and mNG, to assess the exocytosis activity at the
209 damage site. The accumulation of Myo2-sfGFP and Exo70-mNG at the damage site was impaired
210 in *sla1*Δ, *end3*Δ, and *vrp1*Δ (Fig. 4, A and B, fig. S6, A and B). Moreover, we also found that the
211 dispersion of Myo2-sfGFP and Exo70-mNG from the bud tip was partially inhibited in CME
212 mutants (Fig. 4, A and B, fig. S6, A and B). The observed weak phenotype of *rvs167*Δ for the
213 accumulation and dispersion of Myo2-sfGFP and Exo70-mNG is consistent with the previous
214 study that exocytosis is not impaired in *rvs167*Δ (47).
215 Our previous work also showed that the actin nucleator formin Bni1 and the exocyst subunit Sec3
216 are degraded in response to SDS treatment (26). To test the possibility that CME is required for
217 the decrease of Bni1 and Sec3 after SDS treatment, we performed immunoblotting of Bni1-
218 13xMyc and Sec3-GFP before and after SDS treatment (Fig. S7, A and B). Protein levels of Bni1-
219 13xMyc and Sec3-GFP were decreased in WT, *rvs167*Δ, and *end3*Δ after SDS treatment (Fig. S7,
220 A and B). Given that *end3*Δ impaired the accumulation of Myo2-sfGFP and Exo70-mNG at the
221 damage site (Fig. 4, A and B), these results suggest that CME is dispensable for the decrease of
222 Bni1 and Sec3 after SDS treatment. Altogether, these results suggest that CME is involved in the
223 direction of the Exo70-mNG and Myo2-sfGFP to the damage site in a Bni1- and Sec3-
224 degradation-independent manner.
225
226 **CME at the bud tip directs repair proteins with TMDs to the damage site**
227 Although the requirement of Rvs167 for the Pkc1 accumulation and polarized exocytosis at the
228 damage site is minimal (Fig. 4, A to C), *rvs167*Δ is sensitive to SDS (Fig. S5C). This raised the
229 possibility that CME plays additional roles, such as membrane protein trafficking, in PM repair.
230 We found that CME proteins, including Apl1, Ede1, and Ent1, changed their localization from the
231 bud neck to the bud tip within 10 min after laser damage (Fig. S8A). The fluorescence intensity
232 changes of CME proteins at the bud tip at 10 min after laser damage were higher than those of
233 other repair protein candidates (Fig. S8B). Consistent with these results, the Ede1-mSc-I signal at
234 the bud tip increased within 10 min after laser damage, and then the Ede1-mSc-I signal at the
235 damage site increased (Fig. 5A). These results suggest that CME occurs at the bud tip within 10
236 min after laser damage. We also found that Dnf1-mNG disappeared from the bud tip following
237 the recruitment of Ede1-mSc-I to the bud tip (Fig. 5, A and B). The disappearance from the bud
238 tip and the accumulation at the damage site of Dnf1-mNG were impaired in *rvs167*Δ (Fig. 5, B
239 and C, and fig. S9). Furthermore, the disappearance from the bud tip and the accumulation at the
240 damage site of repair proteins with TMDs (Slg1-sfGFP and Sho1-GFP) and representative
241 endocytic recycling cargo, mNG-Snc1, were impaired in *rvs167*Δ (Fig. 5, D to F and fig. S10, A
242 to C). These results support our idea that CME directs repair proteins with TMDs from the bud tip
243 to the damage site.
244
245 **mNG-Snc1 is retargeted from the damage site to the bud tip**

246 The fluorescence intensity of accumulated repair proteins with TMDs at the damage site gradually
247 decreases approximately 15 min after laser damage (Fig. 3D and fig. S10, A and C). Using mNG-
248 Snc1 as a model, we investigated the destination of repair proteins after PM repair. To observe the
249 same fraction of mNG-Snc1 before and after laser damage, we transiently expressed mNG-Snc1
250 under the control of the galactose-inducible promoter (Gal1pr) for 1 hour (Fig. 6A). Then, we
251 transferred the cells to glucose media to stop the expression (Fig. 6A). To minimize the effect of
252 changing the carbon source, we further incubated the cells in glucose media for at least 3 hours
253 prior to laser damage (Fig. 6A). The mNG-Snc1 accumulated at the damage site approximately
254 ~10 min after laser damage, gradually disappearing after the colocalization with Ede1-mSc-I (Fig.
255 6A and B). The mNG-Snc1 signal at the bud tip decreased to 10-53% 22 min after laser damage
256 (Fig. 6C and D). The normalized mNG-Snc1 signal at the bud tip recovered to 54-88% 50 min
257 after laser damage. (Fig. 6, C and D). These results suggest that mNG-Snc1 is redirected to the
258 bud tip after PM repair.
259
260 **Discussion**
261 There has been a growing interest in the mechanisms underlying PM repair, partly due to their
262 association with human diseases and cellular aging (3-5, 28). PM repair proteins, which
263 accumulate at the damage site, play critical roles in PM repair. In this study, by large-scale
264 identification of PM repair proteins and single- and dual-color live-cell imaging of repair proteins,
265 we analyzed spatiotemporal PM repair processes in budding yeast. We propose a model in which
266 CME at the bud tip and at the damage site delivers repair proteins with TMDs between the bud tip
267 and the damage site, allowing the cell to restructure the damaged PM and to resume growth after
268 PM repair (Fig. 7).
269
270 **Two-step visual screening for PM repair protein identification**
271 By combining proteome-scale visual screening using yeast GFP libraries and the laser damage
272 assay, we identified 80 repair protein candidates (Fig. 2B and Data S2). Strikingly, 72 out of 80
273 repair protein candidates were not previously reported to accumulate at the damage site in
274 budding yeast (26, 27). The unreported repair protein candidates include uncharacterized proteins,
275 such as Sap1 and Ypr089w (Data S2). Characterizing these proteins may expand our
276 understanding of PM repair mechanisms.
277 We selected the screening hits from the C-terminally GFP-tagged library as targets for the laser
278 damage assay. Although this is a reasonable approach to evaluating the proteins from the
279 endogenous expression level, it overlooks the potential repair proteins in the N-terminally sfGFP-
280 tagged library. Around 23% of ORFs only exist in the N-terminal library, and 11% of yeast ORFs
281 show different localization from that of the C-terminal library (31). For example, sfGFP-Snc2, but
282 not Snc2-GFP, changes localization in response to SDS treatment because of the mislocalization
283 of Snc2-GFP in the vacuole. Because Snc2 is a homolog of Snc1, Snc2 is a potential repair
284 protein. Screening hits from the N-terminally sfGFP-tagged library can also be a useful resource
285 for further identification of repair proteins.
286 The screening is unable to identify proteins whose localization remains unaltered in response to
287 SDS treatment. For example, we could not identify Cdc50-Drs2, which accumulates at the
288 damage site induced by a laser (27). A recent study demonstrated the different cellular responses
289 between focal (laser damage) and diffuse (streptolysin-O (SLO) treatment) PM damages (6).
290 Some proteins may be overlooked in the screening due to the intrinsic differences between SDS
291 treatment and the laser damage assay. In addition, the screening did not identify ESCRT proteins
292 as hits. The tagging of fluorescent proteins occasionally interferes with the functions of the tagged
293 proteins (48). Specifically, the exogenous expression of fluorescent-tagged ESCRT subunits can
294 impair their functions (49, 50). The screening may have overlooked some of these proteins,
295 possibly including ESCRT proteins.

296 We performed live-cell imaging of repair proteins and defined accumulation times of repair
297 proteins (Fig. S2 and Data S2). This dataset provides an overview of repair protein accumulation.
298 However, it should be noted that the accurate relative accumulation timing of repair proteins
299 should be determined by multi-color imaging of repair proteins in the same cells, because of cell-
300 cell variabilities, the GFP-tagging effects on the cells, and small sample size of the screening.
301 These datasets will form the basis for future hypothesis-driven studies.
302
303 **Coordination of polarized exocytosis and CME**
304 We showed that polarized exocytosis and CME occur simultaneously at the damage site between
305 approximately 5 and 35 min after laser damage (Fig. 3, C and D). Given that the resealing of the
306 damaged PM generally occurs within 1 min (20), this result implies that polarized exocytosis and
307 CME are involved in the restructuring of the damaged PM rather than the resealing of it. The
308 coupling of endocytosis with polarized exocytosis is observed in multiple cell types, including at
309 the growing tip of budding yeast, the growing tip of pollen tubes, and synapses in neurons (51).
310 Polarized exocytosis and CME at the damage site may regulate the PM tensions and amount of
311 lipids and PM proteins in a manner analogous to these cells.
312 Our results suggest that the activity of CME and polarized exocytosis at the damage site changes
313 over time, with exocytosis predominating within 20 min after laser damage and CME
314 predominating 20 min after laser damage (Fig. 3, C and D). This is consistent with the recent
315 study in human cells (21). A previous study showed that polarized exocytosis activates CME in
316 budding yeast (47). Rab GTPase Sec4, which regulates polarized exocytosis, also activates
317 endocytosis by overriding Sla1 inhibition of Las17 (47). We could not identify Sec4 as a repair
318 protein candidate because C-terminally GFP-tagged Sec4 is not in the library, probably due to the
319 loss of function of C-terminally tagged Sec4. However, we found that Sec2-GFP, the guanine
320 nucleotide exchange factor (GEF) of Sec4, accumulates at the damage site (Data S2). Sec4 and
321 Sec2 are localized to the secretory vesicles (52, 53). Therefore, secretory vesicles that are targeted
322 to the damage site may accumulate Sec2 and Sec4, leading to the activation of CME. The
323 switching of activities between polarized exocytosis and CME may contribute to restoring PM
324 homeostasis after the damage.
325 Polarized exocytosis at the damage site is inhibited in CME mutants (Fig. 4, A and B, and fig. S6,
326 A and B). Given that CME and polarized exocytosis occur simultaneously (Fig. 3, C and D),
327 CME may activate polarized exocytosis at the damage site, such as by regulating the PM tension
328 (54) around the damage site. Moreover, Myo2-sfGFP and Exo70-mNG were partially retained at
329 the bud tip after laser damage in CME mutants (Fig. 4, A and B, and fig. S6, A and B). These
330 results raise the possibility that CME is involved in targeting Exo70 and Myo2 from the bud tip.
331 At the bud tip, CME may be involved in the dispersion of Exo70 and Myo2 via upstream
332 regulators, such as Rho3.
333
334 **CME functions for PM repair in budding yeast**
335 Previous studies showed that endocytosis actively occurs at the damage site to repair the damaged
336 PM (11, 12, 20). Surprisingly, our results suggest that CME occurs not only at the damage site but
337 at the bud tip within 10 min after laser damage. In *rvs167*Δ, in which exocytosis inhibition at the
338 damage site is minimal (Fig. 4, B and C), repair proteins with TMDs at the bud tip fail to
339 accumulate at the damage site (Fig. 5, B to F). These results are consistent with our idea that
340 CME at the bud tip directs repair proteins with TMDs to the damage site (Fig. 7). Consistent with
341 our results, dysferlin-containing vesicles increase in response to PM damage in muscle cells (25,
342 55). Dysferlin has a TMD and functions as a PM repair protein (25, 55, 56). Delivery of repair
343 proteins with TMDs from non-damaged sites to the damage site by endocytosis may occur in a
344 wide range of eukaryotic species.

345 We showed that 54-88% of the normalized mNG-Snc1 signal at the bud tip is recovered 50 min
346 after the damage (Fig. 6, C and D). Because Snc1 is a CME cargo and it colocalizes with Ede1-
347 mSc-I at the damage site, it is presumably recovered from the damage site via CME. Previous
348 studies showed that macropinocytosis and CME restructure the damaged PM in human cells (20,
349 21). However, it is not clear whether the cargo proteins are recycled or degraded. We propose that
350 CME terminates the PM damage responses by removing the repair proteins with TMDs from the
351 damage site and resuming the growth by retargeting them to the bud tip (Fig. 7).
352
353 Here, we showed spatiotemporal cellular responses after PM damage in budding yeast by large-
354 scale identification of repair proteins and their live-cell imaging. Despite the limitations
355 mentioned above, our datasets provide the first functional catalog for PM repair proteins. Because
356 some of the PM repair proteins identified in this study and CME mechanisms are evolutionarily
357 conserved, this work may serve as a basis for future studies, including those to be conducted in
358 mammalian cells.
359
360 **Materials and Methods**
361 **Media and strains**
362 Standard procedures were used for DNA, *E. coli*, and yeast genetic manipulation. Yeast
363 transformations were performed using the lithium acetate method. A PCR-based procedure was
364 used for gene deletion. The deletion of the expected locus was confirmed by colony PCR (57).
365 Yeast cells were cultured in YPD media (1% yeast extract, 2% bacto peptone, and 2% glucose)
366 unless otherwise indicated. SD media (yeast nitrogen base (6.7 g/liter) without amino acids, L-
367 adenine (550 mg/liter), L-arginine (280 mg/liter), L-alanine (280 mg/liter), L-asparagine (280
368 mg/liter), L-aspartic acids (280 mg/liter), L-cysteine (280 mg/liter), glycine (280 mg/liter), L–
369 glutamic acids (280 mg/liter), L-glutamine (280 mg/liter), L-isoleucine (280 mg/liter), L-lysine
370 (280 mg/liter), L-phenylalanine (280 mg/liter), L-proline (280 mg/liter), L-serine (280 mg/liter), L-
371 threonine (280 mg/liter), L-tyrosine (280 mg/liter), L-valine (280 mg/liter), leucine (530 mg/liter),
372 methionine (86 mg/liter), histidine (86 mg/liter), uracil (22 mg/liter), myo-inositol (100 mg/liter),
373 and *p*-aminobenzoic acid (3 mg/liter) (pH 5.5)) were used for the laser damage assay. Yeast
374 culture was performed at 25°C unless otherwise indicated. The yeast strains, yeast libraries, and
375 plasmids used in this study are listed in Tables S1 to S3.
376 For the mNG-Snc1 expression experiments in Fig. 6, we grow cells in SD media containing 2%
377 raffinose instead of glucose overnight. Then, we induced the expression of mNG-Snc1 by adding
378 3% galactose. After one hour of growth in galactose media, the cells were centrifuged at 5000xg
379 for 5 min, and the spun-down cells were washed twice with SD media containing 2% glucose. We
380 transferred the spun-down cells to SD media containing 2% glucose. The cells were incubated for
381 at least 3 hours before the laser damage assay.
382
383 **GFP screen for SDS damage response**
384 GFP strains were spotted onto the YPD plates from 96-well plates using a pin replicator and
385 incubated at 25°C. After 3 days, the colonies were inoculated into 200 µl of YPD media and
386 incubated overnight to saturation. After mixing, 3 µl of the saturated culture was transferred to 1
387 ml of YPD media in deep well plates and incubated for 4-5 hours. 500 µl of the cultures were
388 transferred to the new deep well plates. 10 µl of 1% SDS was added to 500 µl of the cultures and
389 incubated at 25°C for 1 hour. The cells were centrifuged at 2000xg for 2 min. The cells were fixed
390 by 300 µl of 4% PFA in YPD for 30 min at room temperature. The fixed cells were centrifuged at
391 2000xg for 2 min. Cells were washed twice with PBS and centrifuged at 2000xg for 2 min. The
392 supernatant was removed between each wash. Cells were kept at 4°C until imaging. Cells were
393 imaged with an LSM880 confocal microscope using a 20x air objective lens with an airyscan

394 detector for GFP fluorescence (Ex 488/Em522). Maximum intensity projections of z-stack images
395 are shown.
396
397 **Categorization of localization changes in response to SDS treatment**
398 We manually reviewed the acquired images using Zen Blue edition (Zeiss) or Fiji software (58)
399 and compared the fluorescence signals of GFP-tagged proteins in normal and SDS treatment
400 conditions. We identified the proteins whose fluorescence signal pattern changes between the two
401 conditions. We categorized the screening hits based on reported protein localization (29). We first
402 categorized the bud tip- or the bud neck-localizing proteins as "From bud tip/neck". Among the
403 uncategorized remaining screening hits, the actin-localizing proteins were categorized as "Actin".
404 Among the remaining uncategorized screening hits, cell periphery-localizing proteins were
405 categorized as "From cell periphery." Among the remaining uncategorized screening hits,
406 nucleus-localizing proteins were categorized as "Nucleus" or "Nucleus to the cytoplasm". We
407 categorized Urc1 as "Nucleus to cytoplasm" because its signal dispersed to the cytoplasm in an
408 SDS treatment condition. Other proteins in the "Nucleus" showed stronger nucleus localization in
409 the SDS treatment conditions. Among the remaining uncategorized screening hits, we categorized
410 mitochondria-localizing proteins as "Mitochondria". Among the remaining uncategorized
411 screening hits, we categorized spindle pole-localizing proteins as "Spindle pole." All proteins in
412 the "Spindle pole" showed stronger dot-like structures in the SDS treatment condition. Among the
413 remaining uncategorized screening hits, we categorized proteins that show puncta or foci in SDS
414 treatment conditions as "Puncta/foci." We categorized Gcn2, Ato3, Sun4, Csi2, Sps4, and
415 Ypr089w as "Puncta/foci dispersed" because they showed weaker foci or puncta signals in SDS
416 treatment conditions. We categorized Tul1, Emp24, Hor7, Scw10, and Ynl019c as "From
417 vacuole" because they showed decreased vacuole signal in the SDS treatment conditions. We
418 categorized Prm5 as "to vacuole" because its vacuole signal increases. We categorized Yps1 and
419 Msc1 as "cytoplasm to ER" because they localize to the ER, and their ER signal increased in SDS
420 treatment conditions. In this study, we make use of the protein localization data from the
421 Saccharomyces Genome Database (SGD) and (29). All results of this screening are shown in Data
422 S1.
423
424 **Laser damage assay**
425 Yeast cells were grown in SD medium at 25°C until the culture reached an OD600 of 0.1-0.4. We
426 diluted the yeast culture and further incubated the yeast cells in SD medium for 3-8 hours at 25˚C.
427 We took 1 mL of the culture and centrifuged it at 500xg for 5 min to spin the cells down. We took
428 5-10 µL of the cell suspension and placed it onto SD medium + 2.2% agarose bed. A
429 Concanavalin A (ConA) (Nacalai Tesque) coated glass slip was placed on the cells prior to
430 imaging.
431 Cells were observed with A1R (Nikon). A1R was equipped with a CFI Apochromat TIRF
432 60×/1.49 oil objective lens (Nikon). GFP, mNG, and sfGFP were excited by a 488 nm laser, and
433 the fluorescence that passed a 525/50 nm band-pass filter was detected with a GaAsP detector.
434 mSc-I was excited by a 561 nm laser, and the fluorescence that passed a 595/50 nm band-pass
435 filter was detected with a GaAsP detector. For the laser damage assay, the 405 nm laser was
436 irradiated to a circle of 0.5 µm diameter in a cell periphery. The laser power was set between 30%
437 and 70%, depending on the fluorescence-tagged proteins. We determined the laser power
438 sufficient for repair protein recruitment at the damage site in control cells without resulting in cell
439 lysis during the experiments. At least ~80% of cells are viable during the experiments, otherwise
440 indicated. Only the cells that survive after laser damage are quantified. To compare the
441 accumulation of repair proteins between different strains, we set the exact same laser power and
442 microscopy.
443

444 **Categorization of localization changes in response to laser damage**
445 We categorized proteins that accumulate at the damage site as “Damage site”. These proteins are
446 defined as repair protein candidates. Among the remaining uncategorized proteins, we categorized
447 cell periphery-localizing proteins as “PM to cytoplasm”. Among the remaining uncategorized
448 proteins, we categorized Msn2 and Crz1 as "Nucleus" because they changed localization from the
449 cytoplasm to the nucleus. Among the remaining uncategorized proteins, we categorized Dot6,
450 Dna2, Msc1, and Gcd7 as "Puncta" because they formed punctate structures in response to laser
451 damage. The repair protein candidates identified in this study are listed in Data S2.
452
453 **Quantification of fluorescence signal for laser damage assay**
454 The quantification of the fluorescence signal from the laser damage assay was performed as
455 described previously (27). For the large-scale identification of repair protein candidates, we
456 selected the region of interest (ROI) around the whole cell, the damage site, and the bud tip of the
457 cells. We manually move the ROIs as the cell moves so that the ROIs remain at the same position
458 in the cell. We set the ROIs and manually selected them for quantification. The fluorescence
459 intensity at the damage site and the bud tip were normalized by the fluorescence intensity of a
460 whole cell to minimize the effect of photobleaching during imaging.
461 We defined the accumulation time as the time when the fluorescence intensity at the damaged site
462 became greater than the fluorescence intensity at the non-damaged site by three times the standard
463 deviation (3xSD) for at least two consecutive time frames. We defined the dispersion time when
464 the fluorescence intensity at the damage site becomes less than that of the non-damaged site plus
465 3xSD for at least two consecutive time frames after the accumulation time. We defined the
466 retention time as the difference between the accumulation time and the dispersion time. We
467 measured at least three cells. The median values of accumulation times and retention times across
468 replicates for all repair proteins are listed in Data S2.
469
470 **Growth screening of repair protein knockout mutants**
471 Yeast cultures grown overnight in YPD at 25°C were diluted to OD600 = 0.1. The diluted
472 cultures were spotted onto YPD, YPD + 0.01% SDS, and YPD + 25 μg/ml CFW plates. After 3
473 days of incubation at 25°C or 37°C (Heat stress), the growth of the YPD plate and other plates
474 was compared. We performed the screening of two independent colonies. The strains were from
475 the yeast deletion collection library (59) except for *smi1*Δ, *las17*Δ, *skg6*Δ, *end3*Δ, *vrp1*Δ, and
476 *sla2*Δ. Only the mutants that showed sensitivity to the stress in two independent colonies were
477 defined as sensitive to the stress. The results of the screening are shown in Data S2.
478
479 **Spot assay**
480 Yeast cultures grown overnight in YPD at 25°C were diluted to OD600 = 0.1. The four-fold serial
481 dilutions of cultures were spotted onto the indicated plates.
482
483 **Immunoblotting**
484 Yeast cells in the early log phase (OD600 = 0.1-0.3) were treated with 0.02% SDS. 5 ml of yeast
485 cells were collected before SDS treatment, 1 hr after SDS treatment, and 2 hr after SDS treatment.
486 Cells were flash frozen by liquid nitrogen and stored at -80°C. Cells were resuspended in 120μl of
487 cold lysis buffer (0.25 M NaOH and 1% β-mercaptoethanol) and incubated on ice for 10 min. 20
488 μl of trichloroacetic acid was added to the lysates. After 10 min of incubation on ice, the lysates
489 were spun down, and the supernatant was discarded. The precipitates were washed with 500μl
490 ice-cold acetone twice and dried at room temperature. The precipitates are resuspended in SDS
491 polyacrylamide gel electrophoresis (PAGE) sample buffer [63 mM tris-Cl (pH 6.8), 2% SDS, 1%
492 β-mercaptoethanol, 0.01% Bromophenol Blue, and 10% glycerol]. Immunoblotting was

performed with anti-mini c-Myc (SANTA CRUZ, sc-40), anti-GFP (Roche Merck, 11814460001), or anti-tubulin α (Bio-Rad, MCA78G) antibodies.

Statistical Analysis

Dunnett's multiple comparison test, Welch's t-test, and Mann–Whitney U test were performed with Python software (v. 3.11). Gene enrichment analysis and Fisher's exact test were performed with R software (v. 4.2.2).

References

1. P. L. McNeil, T. Kirchhausen, An emergency response team for membrane repair. *Nature reviews. Molecular cell biology* **6**, 499-505 (2005).
2. C. Dias, J. Nylandsted, Plasma membrane integrity in health and disease: significance and therapeutic potential. *Cell Discov* **7**, 4 (2021).
3. R. Bashir *et al.*, A gene related to Caenorhabditis elegans spermatogenesis factor fer-1 is mutated in limb-girdle muscular dystrophy type 2B. *Nat Genet* **20**, 37-42 (1998).
4. J. Suzuki, M. Umeda, P. J. Sims, S. Nagata, Calcium-dependent phospholipid scrambling by TMEM16F. *Nature* **468**, 834-838 (2010).
5. N. Wu *et al.*, Critical Role of Lipid Scramblase TMEM16F in Phosphatidylserine Exposure and Repair of Plasma Membrane after Pore Formation. *Cell reports* **30**, 1129-1140 e1125 (2020).
6. D. C. Bittel, J. K. Jaiswal, Early Endosomes Undergo Calcium‐Triggered Exocytosis and Enable Repair of Diffuse and Focal Plasma Membrane Injury. *Advanced Science* **10** (2023).
7. N. Raj *et al.*, Early Endosomes Act as Local Exocytosis Hubs to Repair Endothelial Membrane Damage. *Advanced Science* **10**, 2300244 (2023).
8. A. Reddy, E. V. Caler, N. W. Andrews, Plasma Membrane Repair Is Mediated by Ca2+-Regulated Exocytosis of Lysosomes. *Cell* **106**, 157-169 (2001).
9. G. Q. Bi, J. M. Alderton, R. A. Steinhardt, Calcium-regulated exocytosis is required for cell membrane resealing. *Journal of Cell Biology* **131**, 1747-1758 (1995).
10. K. Miyake, P. L. McNeil, Vesicle accumulation and exocytosis at sites of plasma membrane disruption. *Journal of Cell Biology* **131**, 1737-1745 (1995).
11. V. Idone *et al.*, Repair of injured plasma membrane by rapid Ca2+-dependent endocytosis. *The Journal of Cell Biology* **180**, 905-914 (2008).
12. C. Tam *et al.*, Exocytosis of acid sphingomyelinase by wounded cells promotes endocytosis and plasma membrane repair. *J Cell Biol* **189**, 1027-1038 (2010).
13. A. J. Jimenez *et al.*, ESCRT Machinery Is Required for Plasma Membrane Repair. **343**, 1247136 (2014).
14. L. L. Scheffer *et al.*, Mechanism of Ca2+-triggered ESCRT assembly and regulation of cell membrane repair. *Nature Communications* **5**, 5646 (2014).
15. C. A. Mandato, W. M. Bement, Actomyosin transports microtubules and microtubules control actomyosin recruitment during Xenopus oocyte wound healing. *Curr Biol* **13**, 1096-1105 (2003).
16. W. M. Bement , H. l. n. A. Benink , G. von Dassow A microtubule-dependent zone of active RhoA during cleavage plane specification. *Journal of Cell Biology* **170**, 91-101 (2005).
17. M. T. Abreu-Blanco, J. M. Verboon, S. M. Parkhurst, Cell wound repair in Drosophila occurs through three distinct phases of membrane and cytoskeletal remodeling. *J Cell Biol* **193**, 455-464 (2011).
18. H. A. Benink, W. M. Bement, Concentric zones of active RhoA and Cdc42 around single cell wounds. *J Cell Biol* **168**, 429-439 (2005).

543 19. M. L. Ebstrup, C. Dias, A. S. B. Heitmann, S. L. Sønder, J. Nylandsted, Actin
544 Cytoskeletal Dynamics in Single-Cell Wound Repair. *International journal of molecular*
545 *sciences* **22** (2021).
546 20. S. L. Sønder *et al.*, Restructuring of the plasma membrane upon damage by LC3-
547 associated macropinocytosis. *Science Advances* **7**, eabg1969 (2021).
548 21. N. Raj *et al.*, Membrane Tension Regulation is Required for Wound Repair. *Advanced*
549 *science (Weinheim, Baden-Wurttemberg, Germany)* 10.1002/advs.202402317, e2402317
550 (2024).
551 22. D. A. Ammendolia, W. M. Bement, J. H. Brumell, Plasma membrane integrity:
552 implications for health and disease. *BMC Biology* **19** (2021).
553 23. N. J. Lennon *et al.*, Dysferlin Interacts with Annexins A1 and A2 and Mediates
554 Sarcolemmal Wound-healing. *Journal of Biological Chemistry* **278**, 50466-50473 (2003).
555 24. S. P. Lauritzen, T. L. Boye, J. Nylandsted, Annexins are instrumental for efficient plasma
556 membrane repair in cancer cells. *Semin Cell Dev Biol* **45**, 32-38 (2015).
557 25. J. R. McDade, A. Archambeau, D. E. Michele, Rapid actin-cytoskeleton-dependent
558 recruitment of plasma membrane-derived dysferlin at wounds is critical for muscle
559 membrane repair. *Faseb j* **28**, 3660-3670 (2014).
560 26. K. Kono, Y. Saeki, S. Yoshida, K. Tanaka, D. Pellman, Proteasomal degradation resolves
561 competition between cell polarization and cellular wound healing. *Cell* **150**, 151-164
562 (2012).
563 27. Y. Yamazaki, K. Kono, Clathrin-mediated trafficking of phospholipid flippases is required
564 for local plasma membrane/cell wall damage repair in budding yeast. *Biochemical and*
565 *Biophysical Research Communications* **606**, 156-162 (2022).
566 28. K. Suda *et al.*, Plasma membrane damage limits replicative lifespan in yeast and induces
567 premature senescence in human fibroblasts. *Nature Aging* **4**, 319-335 (2024).
568 29. W.-K. Huh *et al.*, Global analysis of protein localization in budding yeast. *Nature* **425**,
569 686-691 (2003).
570 30. I. Yofe *et al.*, One library to make them all: streamlining the creation of yeast libraries via
571 a SWAp-Tag strategy. *Nat Methods* **13**, 371-378 (2016).
572 31. U. Weill *et al.*, Genome-wide SWAp-Tag yeast libraries for proteome exploration. *Nat*
573 *Methods* **15**, 617-622 (2018).
574 32. T. López-Hernández, V. Haucke, T. Maritzen, Endocytosis in the adaptation to cellular
575 stress. *Cell Stress* **4**, 230-247 (2020).
576 33. S. L. Moon, R. Parker, Analysis of eIF2B bodies and their relationships with stress
577 granules and P-bodies. *Scientific Reports* **8** (2018).
578 34. K. Kono, H. Okada, Y. Ohya, Local and Acute Disruption of the Yeast Cell Surface. *Cold*
579 *Spring Harbor Protocols* **2016**, pdb.prot085266 (2016).
580 35. J. M. Tkach *et al.*, Dissecting DNA damage response pathways by analysing protein
581 localization and abundance changes during DNA replication stress. *Nature Cell Biology*
582 **14**, 966-976 (2012).
583 36. I. Camponeschi, A. Montanari, C. Mazzoni, M. M. Bianchi, Light Stress in Yeasts:
584 Signaling and Responses in Creatures of the Night. *International journal of molecular*
585 *sciences* **24**, 6929 (2023).
586 37. Y. Shimizu, T. Uemura, The sorting of cargo proteins in the plant trans-Golgi network.
587 *Frontiers in Plant Science* **13** (2022).
588 38. M. Kaksonen, C. P. Toret, D. G. Drubin, A modular design for the clathrin- and actin-
589 mediated endocytosis machinery. *Cell* **123**, 305-320 (2005).
590 39. T. Kishimoto *et al.*, Determinants of endocytic membrane geometry, stability, and
591 scission. *Proc Natl Acad Sci U S A* **108**, E979-988 (2011).

40. Y. Sun, N. T. Leong, T. Wong, D. G. Drubin, A Pan1/End3/Sla1 complex links Arp2/3-mediated actin assembly to sites of clathrin-mediated endocytosis. *Molecular Biology of the Cell* **26**, 3841-3856 (2015).
41. R. Lu, D. G. Drubin, Selection and stabilization of endocytic sites by Ede1, a yeast functional homologue of human Eps15. *Molecular Biology of the Cell* **28**, 567-575 (2017).
42. V. Stradalova *et al.*, Distribution of cortical endoplasmic reticulum determines positioning of endocytic events in yeast plasma membrane. *PLoS One* **7**, e35132 (2012).
43. A. F. J. Ram, A. Wolters, R. T. Hoopen, F. M. Klis, A new approach for isolating cell wall mutants in Saccharomyces cerevisiae by screening for hypersensitivity to calcofluor white. *Yeast (Chichester, England)* **10**, 1019-1030 (1994).
44. Z. Török *et al.*, Plasma membranes as heat stress sensors: from lipid-controlled molecular switches to therapeutic applications. *Biochim Biophys Acta* **1838**, 1594-1618 (2014).
45. V. Idone *et al.*, Repair of injured plasma membrane by rapid Ca2+-dependent endocytosis. *J Cell Biol* **180**, 905-914 (2008).
46. L. N. Skalman, M. R. Holst, E. Larsson, R. Lundmark, Plasma membrane damage caused by Listeriolysin O is not repaired through endocytosis of the membrane pore. *Biology Open* **7**, bio035287 (2018).
47. J. Johansen, G. Alfaro, C. T. Beh, Polarized Exocytosis Induces Compensatory Endocytosis by Sec4p-Regulated Cortical Actin Polymerization. *PLOS Biology* **14**, e1002534 (2016).
48. K. Thorn, Genetically encoded fluorescent tags. *Mol Biol Cell* **28**, 848-857 (2017).
49. K. Katoh *et al.*, The ALG-2-interacting protein Alix associates with CHMP4b, a human homologue of yeast Snf7 that is involved in multivesicular body sorting. *J Biol Chem* **278**, 39104-39113 (2003).
50. H. K. Hoffman, M. V. Fernandez, N. S. Groves, E. O. Freed, S. B. van Engelenburg, Genomic tagging of endogenous human ESCRT-I complex preserves ESCRT-mediated membrane-remodeling functions. *J Biol Chem* **294**, 16266-16281 (2019).
51. V. Gerganova, S. G. Martin, Going with the membrane flow: the impact of polarized secretion on bulk plasma membrane flows. *The FEBS Journal* **290**, 669-676 (2023).
52. N. B. Elkind, C. Walch-Solimena, P. J. Novick, The role of the COOH terminus of Sec2p in the transport of post-Golgi vesicles. *J Cell Biol* **149**, 95-110 (2000).
53. R. M. Gingras, A. M. Sulpizio, J. Park, A. Bretscher, High-resolution secretory timeline from vesicle formation at the Golgi to fusion at the plasma membrane in S. cerevisiae. *eLife* **11** (2022).
54. G. Wang, T. Galli, Reciprocal link between cell biomechanics and exocytosis. *Traffic (Copenhagen, Denmark)* **19**, 741-749 (2018).
55. J. R. McDade, M. T. Naylor, D. E. Michele, Sarcolemma wounding activates dynamin-dependent endocytosis in striated muscle. *Febs j* **288**, 160-174 (2021).
56. J. Liu *et al.*, Dysferlin, a novel skeletal muscle gene, is mutated in Miyoshi myopathy and limb girdle muscular dystrophy. *Nature Genetics* **20**, 31-36 (1998).
57. M. S. Longtine *et al.*, Additional modules for versatile and economical PCR-based gene deletion and modification in Saccharomyces cerevisiae. *Yeast (Chichester, England)* **14**, 953-961 (1998).
58. J. Schindelin *et al.*, Fiji: an open-source platform for biological-image analysis. *Nat Methods* **9**, 676-682 (2012).
59. E. A. Winzeler *et al.*, Functional characterization of the S. cerevisiae genome by gene deletion and parallel analysis. *Science* **285**, 901-906 (1999).
60. A. Krogh, B. Larsson, G. von Heijne, E. L. Sonnhammer, Predicting transmembrane protein topology with a hidden Markov model: application to complete genomes. *Journal of molecular biology* **305**, 567-580 (2001).

Acknowledgments
We thank Dr. Maya Schuldiner (Weizmann Institute) for providing the N' SWAT library. We thank Dr. S. Sugiyama for providing yeast strains and technical advice. We also thank the lab members of the Membranology unit for the discussion and critical reading of the manuscript. We are grateful for the help and support provided by the Imaging Section and Sequence Section of the Core Facilities at Okinawa Institute of Science and Technology Graduate University. We thank Dr. P. Barzaghi, Dr. K. Koizumi, Dr. S. Komoto, and Dr. T. Mochizuki for their technical assistance in microscopy experiments.

Funding: This study was supported by MEXT/JSPS KAKENHI Grant Number 23KJ2138 to Y.Y., JSPS grant-in-aid for scientific research (B) 20H03440, 24K02233, and JST-COI-NEXT JPMJPF2205 to K.K..

Author contributions:
Conceptualization, Y.Y. and K.K.; Investigation, Y.Y.; Writing – Original Draft, Y.Y.; Writing – Review & Editing, Y.Y. and K.K.; Funding Acquisition, Y.Y. and K.K.; Supervision, K.K**.**

Competing interests: The authors declare that they have no competing interests.

Data and materials availability: All data needed to evaluate the conclusions in the paper are present in the main text and/or the supplementary materials.

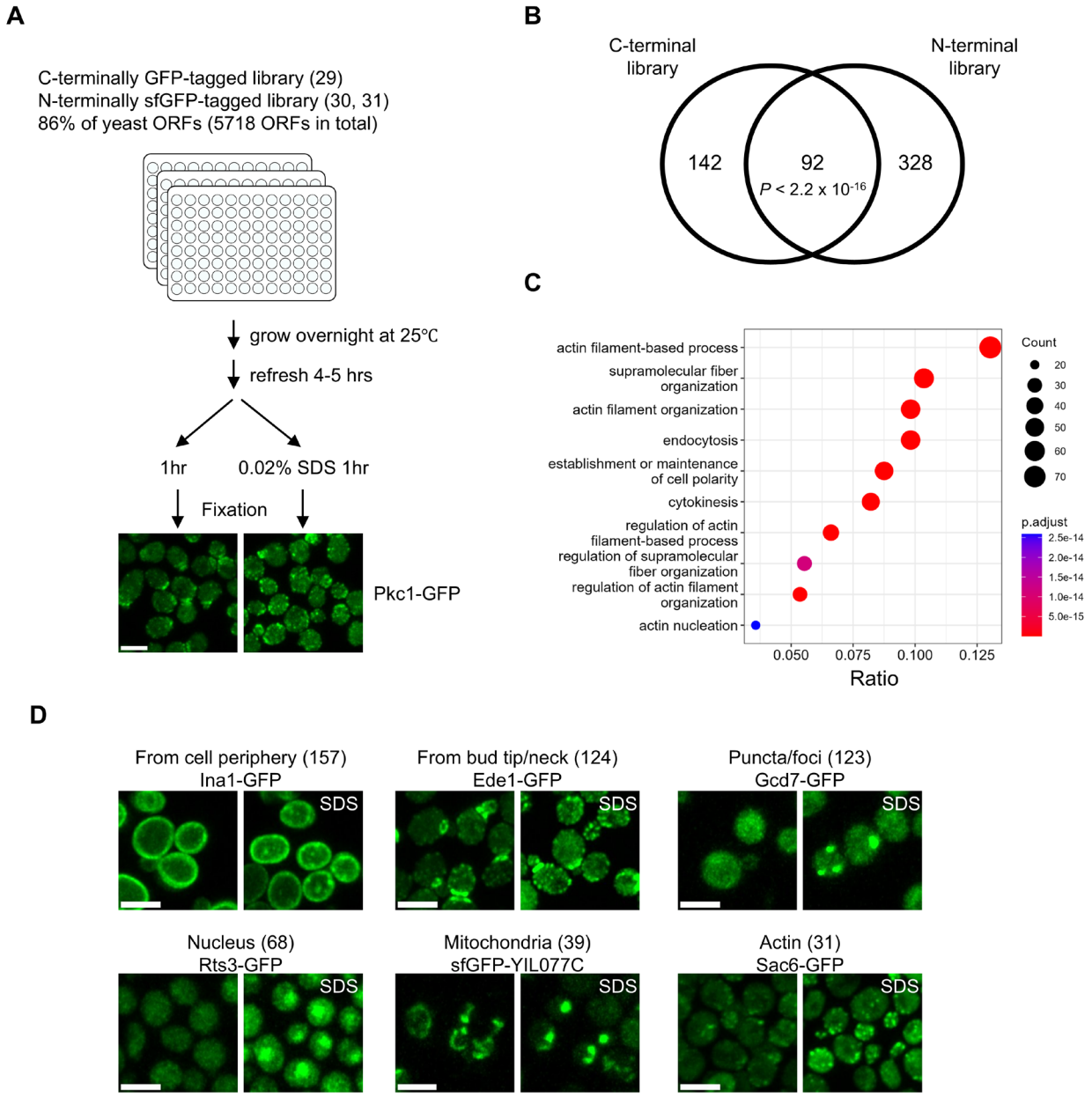

Fig. 1 Protein relocalization in response to SDS treatment.
(A) Schematic representation of screening methodology and images of Pkc1-GFP with or without 0.02 % SDS treatment are shown. Scale bar, 5 µm. **(B)** Overlap of screening hits of C- and N-terminal libraries. P value for the significance of the overlap is indicated. Fisher's exact test was performed. **(C)** GO analysis of biological processes for the screening hits. Successfully observed proteins were used as the background protein sets. **(D)** Screening hits for six relocalization classes and the images of representative proteins in each class were shown. Numbers in parentheses indicate the number of proteins in the class. Scale bar, 2 µm.

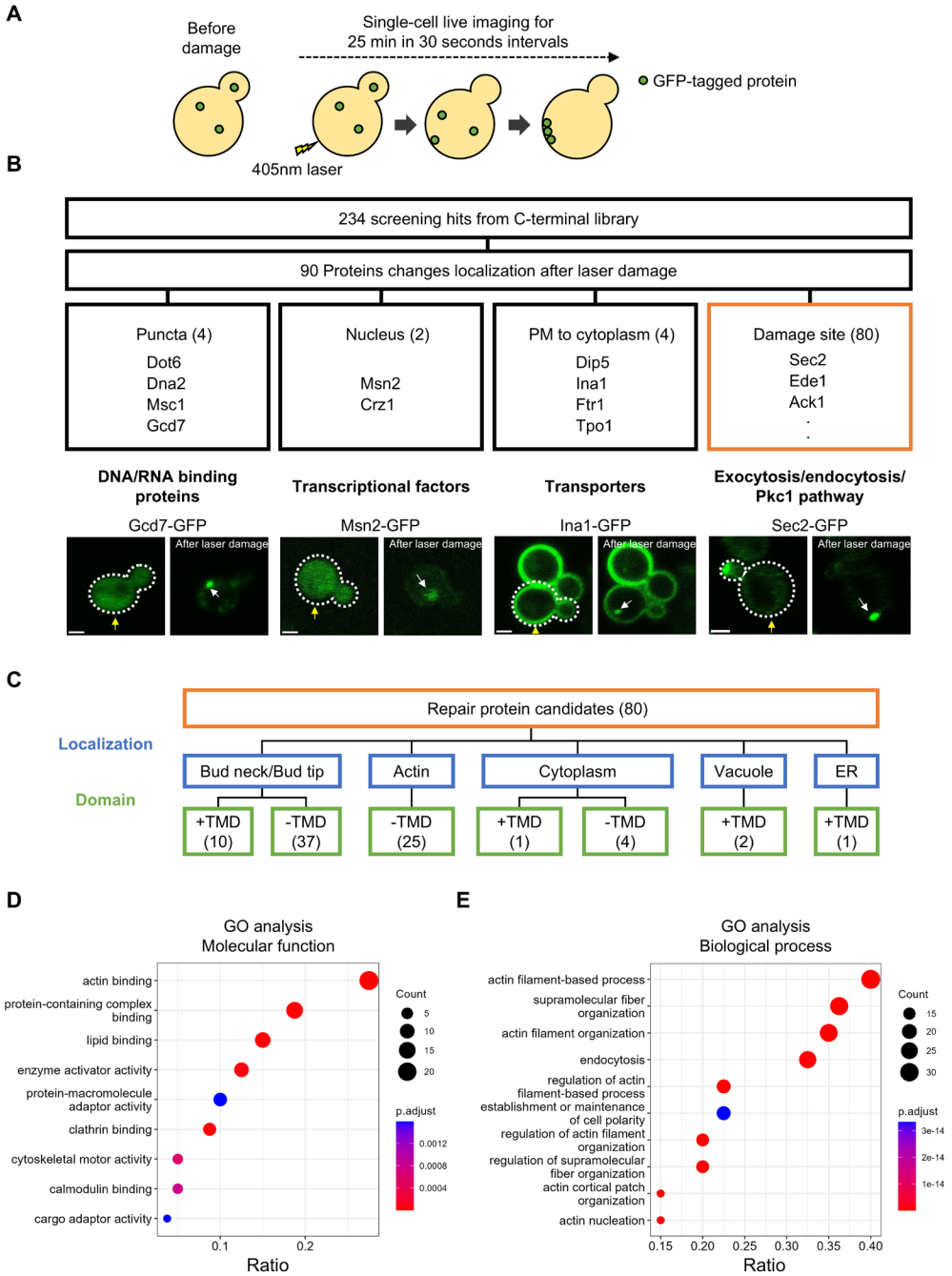

Fig. 2 Laser damage assays identified 80 repair protein candidates. **(A)** Schematic representation of screening methodology. Cells were imaged for 25 min in 30-second intervals after 405 nm laser damage. **(B)** 90 proteins change localization after laser damage. The classification of the repair protein candidates based on their localization changes, representative proteins, and representative biological processes in each category is shown. Scale bar, 2 μm. Yellow arrows show the damage site. White arrows show the recruitment of fluorescence signals. **(C)** Classification of repair protein candidates based on subcellular localization and domain. TMD+ represents the proteins that have transmembrane domains. The existence of transmembrane domains was predicted by TMHMM (60) **(D)** GO analysis of molecular functions for the repair protein candidates. The proteins whose localization changes in response to SDS treatment were used as background protein sets. **(E)** GO analysis of biological processes for the repair protein candidates. The proteins whose localization changes in response to SDS treatment were used as background protein sets.

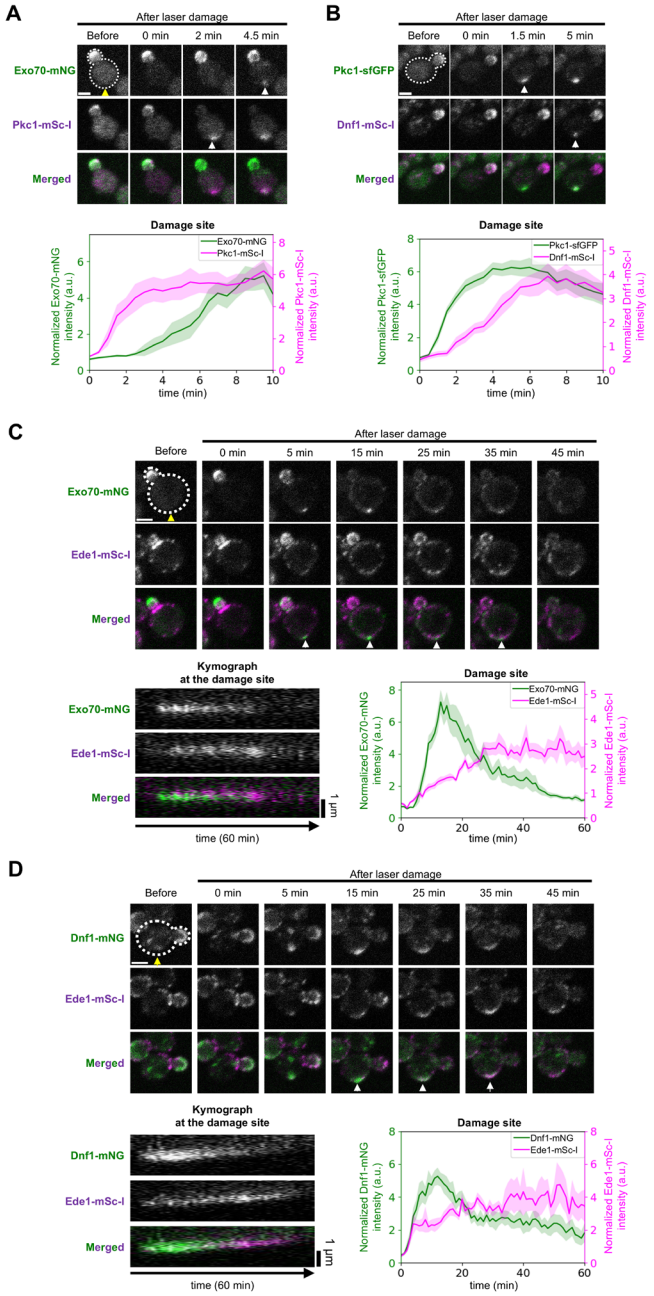

Fig. 3 The temporal order of the Pkc1 accumulation, polarized exocytosis, and CME at the damage site.

(A) The representative images and normalized fluorescence intensity of Exo70-mNG (Green) and Pkc1-mSc-I (Purple) at the damage site after laser damage. Yellow arrows show the damage site. White arrows show the recruitment of fluorescence signals. n = 10 cells. **(B)** The representative images and normalized fluorescence intensity of Pkc1-sfGFP (Green) and Dnf1-mSc-I (Purple) at the damage site after laser damage. Yellow arrows show the damage site. White arrows show the recruitment of fluorescence signals. n = 8 cells. **(C)** Representative images, kymograph at the damage site, and fluorescence intensity at the damage site of Exo70-mNG (Green) and Ede1-mSc-I (purple). n = 10 cells. Yellow arrows show the damage site. White arrows show the coaccumulation of Exo70-mNG and Ede1-mSc-I at the damage site. **(D)** Representative images, kymograph at the damage site, and fluorescence intensity at the damage site of Dnf1-mNG (Green) and Ede1-mSc-I (purple). n = 9 cells. Yellow arrows show the damage site. White arrows show the coaccumulation of Dnf1-mNG and Ede1-mSc-I. Lines and shaded regions are the mean and the standard error of the mean.

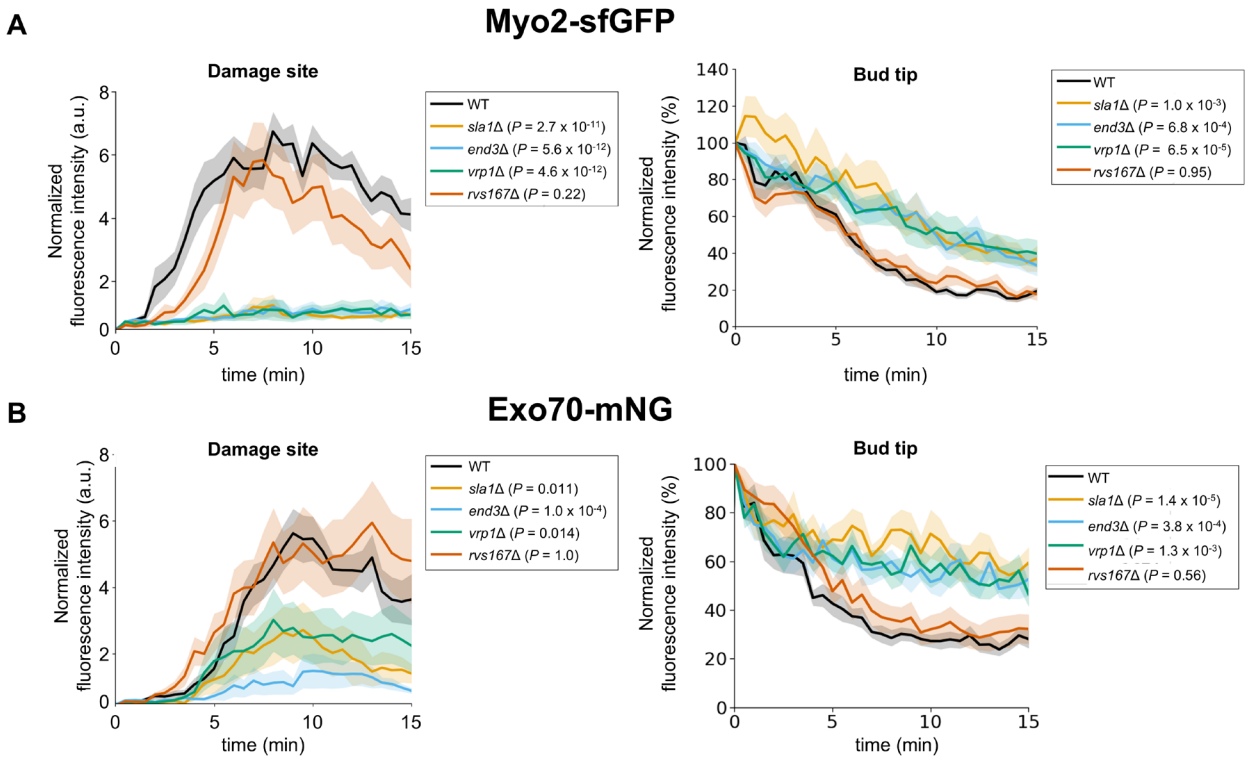

Fig. 4 CME proteins are required for polarized exocytosis at the damage site.
(A) The quantification results of fluorescence intensity of Myo2-sfGFP at the damage site and at the bud tip. n = 13 for WT, n = 12 for *end3*Δ, *sla1*Δ, *rvs167*Δ, and *vrp1*Δ. **(B)** The quantification results of the fluorescence intensity of Exo70-mNG at the damage site. n = 18 for WT, n = 12 for *end3*Δ, *sla1*Δ, and *rvs167*Δ, n = 14 for *vrp1*Δ. Lines and shaded regions are the mean and standard error of the mean. Maximum fluorescence intensity at the damage site or fluorescence intensity changes at the bud tip were compared between WT and mutants using Dunnett's multiple comparison test.

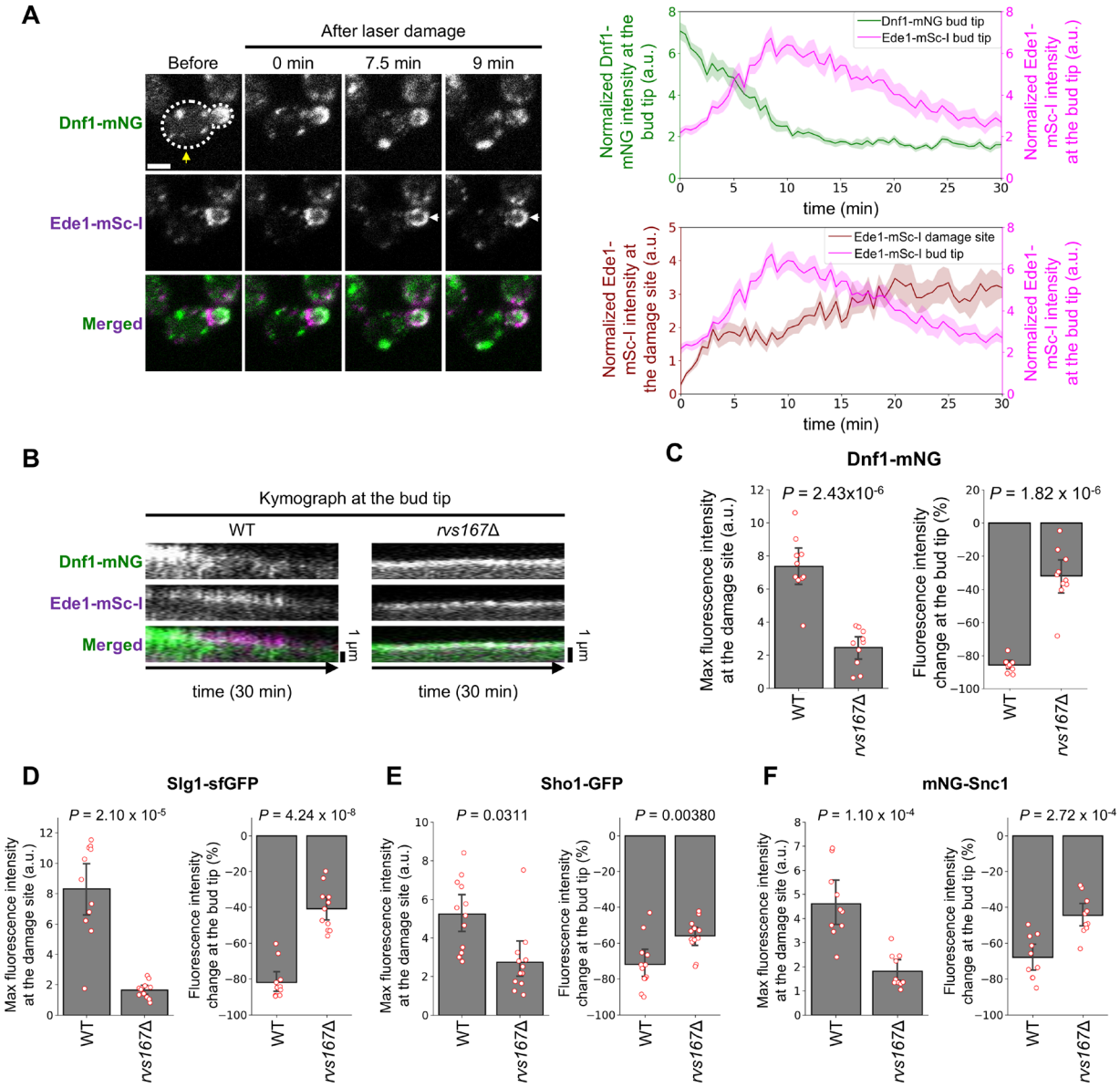

Fig. 5 CME at the bud tip directs repair proteins with TMDs to the damage site. **(A)** Representative images and the normalized fluorescence intensity at the bud tip of Dnf1-mNG and Ede1-mSc-I. Yellow arrows show the damage site. White arrows show the recruitment of fluorescence signals. **(B)** Kymograph of Dnf1-mNG and Ede1-mSc-I at the bud tip in WT and *rvs167*Δ. n = 10 cells. **(C)-(F)** Max fluorescence intensity at the damage site and fluorescence intensity changes at the bud tip in WT and *rvs167*Δ. n = 10 cells for Dnf1-mNG. n = 11 cells for Slg1-sfGFP. n = 12 cells for Sho1-GFP. n = 10 cells for mNG-Snc1. Welch's t-test was performed.

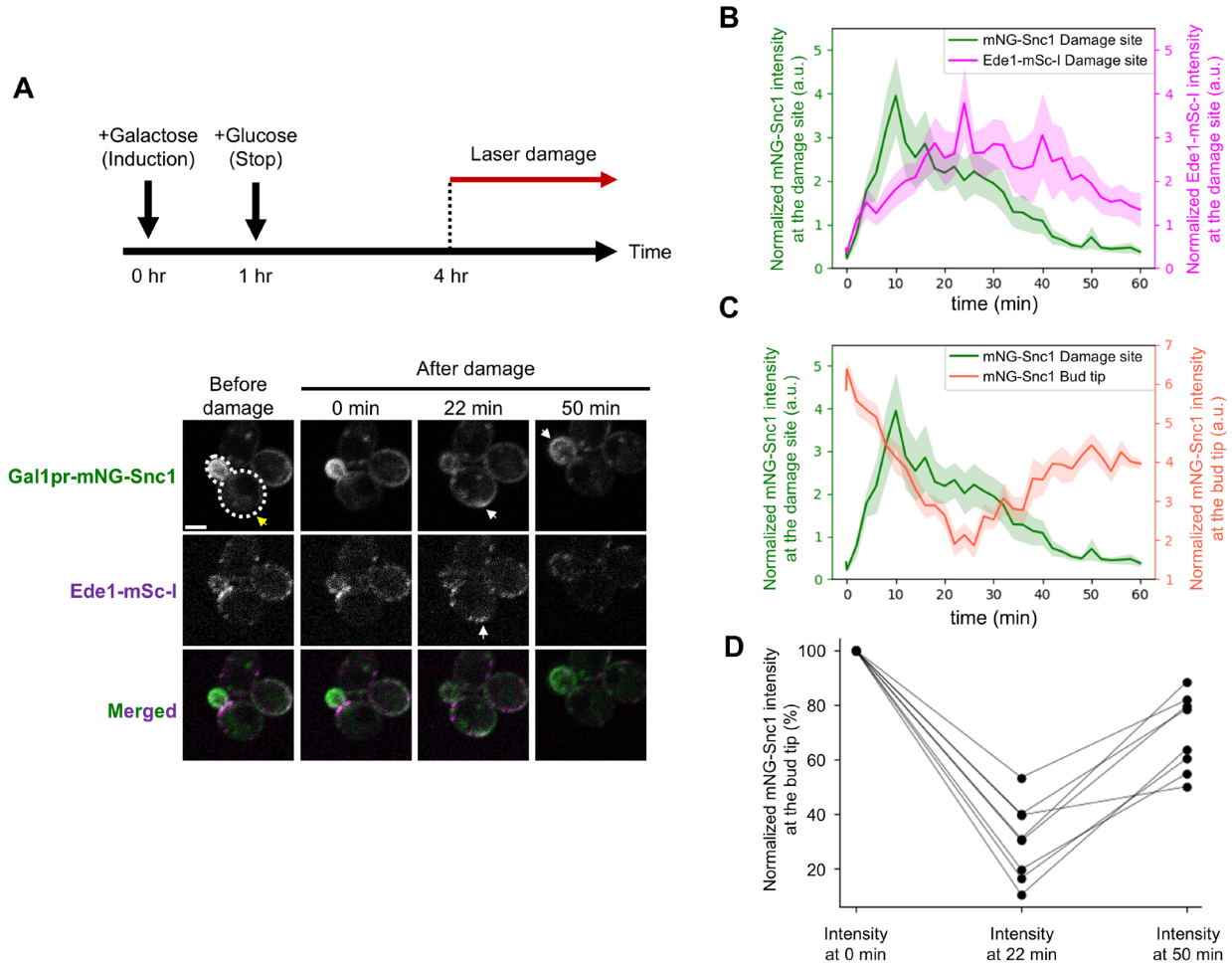

Fig. 6 mNG-Snc1 is recovered from the damage site to the bud tip after PM repair. **(A)** Schematic of transient expression induction of mNG-Snc1 by Gal1 promoter and representative images of mNG-Snc1 and Ede1-mSc-I. After transcription activation of the Gal1 promoter by adding 3% galactose, we stop the expression by transferring the cells to glucose media. The cells were incubated for at least 3 hours before the laser damage assay. Yellow arrows show the damage site. White arrows showed the recruitment of fluorescence signals. **(B)** Quantification of mNG-Snc1 (Green) and Ede1-mSc-I (purple) at the damage site. **(C)** Quantification of mNG-Snc1 at the bud tip (Green) and at the damage site (tomato). **(D)** The changes in the normalized mNG-Snc1 signal at the bud tip. n = 8 cells.

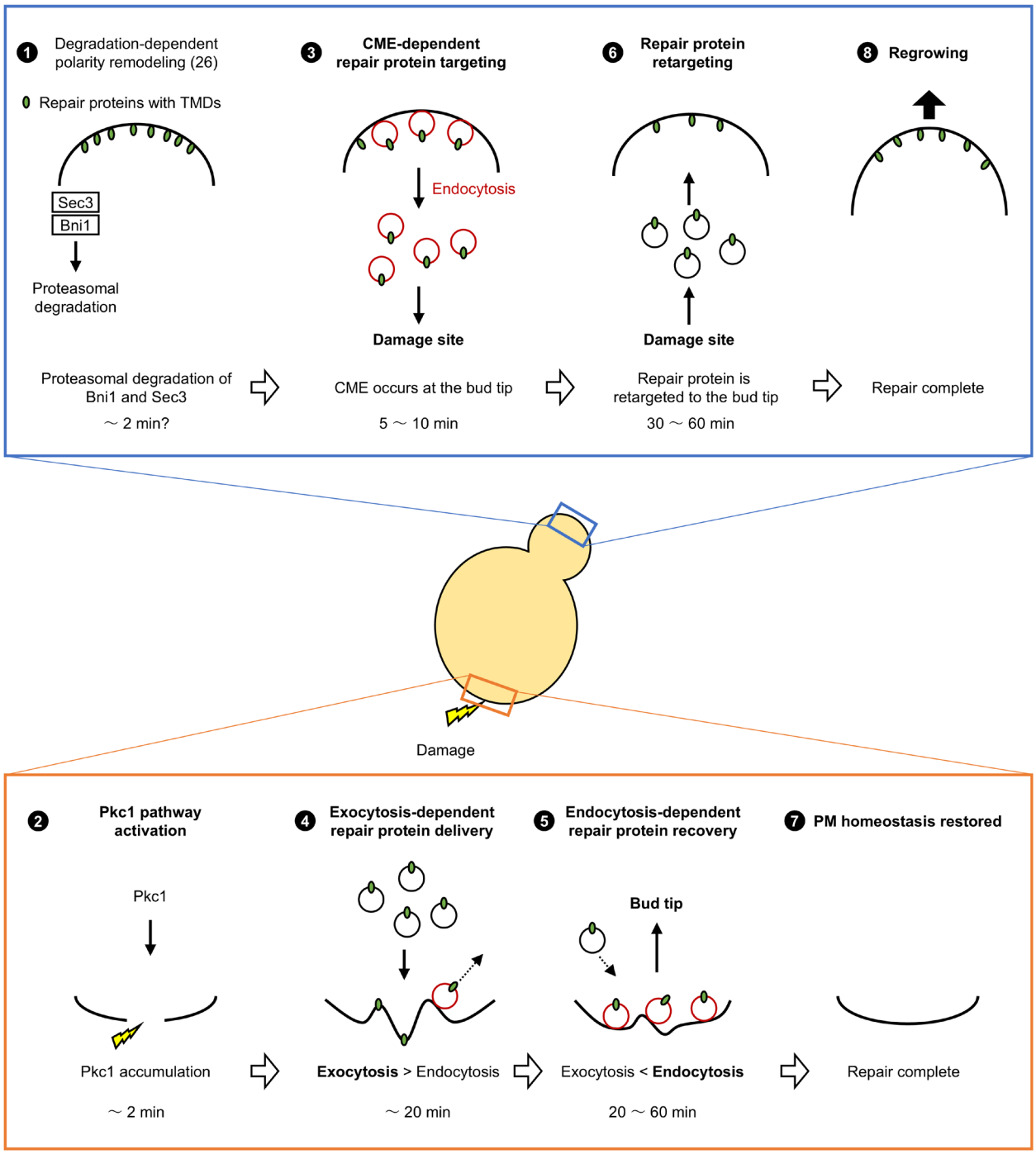

Fig. 7 Model of spatiotemporal cellular responses to PM damage in budding yeast.
We showed the hypothetical model of spatiotemporal PM damage responses in budding yeast. First, the degradation of Sec3 and Bni1 resolved the polarity competition between the bud tip and the damage site (26). Within 10 min after laser damage, CME directs repair proteins with TMDs to the damage site from the bud tip. At the damage site, polarized exocytosis and CME simultaneously occur, with exocytosis predominating approximately within 20 min and with CME predominating approximately 20 min after laser damage. CME targets repair proteins with TMDs from the bud tip to the damage site. The endocytosed PM proteins are retargeted to the bud tip again after the PM repair is finished. The retargeted PM proteins may be involved in the resumption of cell growth after PM repair. The numbers represent the temporal order of events.